Research Article

Anila Ashraf, Muhammad Altaf, Fozia Abasi*, Muhammad Shahbaz, Tanveer Hussain, Md. Arshad Ali, Jaya Seelan Sathiya Seelan, Baber Ali, Maged Mostafa Mahmoud, Steve Harakeh, and Muhammad Hamzah Saleem

Exploring the antimicrobial potential of biogenically synthesized graphene oxide nanoparticles against targeted bacterial and fungal pathogens

Abstract: Graphene oxide (GO) and reduced graphene oxide (rGO) nanoparticles were synthesized using 40 mL of lemon juice extract as a reducing agent. The synthesized nanoparticles were characterized using various analytical techniques, including UV–visible spectroscopy, scanning electron microscopy, energy-dispersive X-ray spectroscopy, Fourier transform infrared spectroscopy, and X-ray diffraction. The results confirmed the successful synthesis of GO and rGO nanoparticles with varied sizes and shapes. The synthesized nanoparticles were tested for their antimicrobial activity against a range of bacterial and fungal strains, including *Escherichia coli*, *Staphylococcus aureus*, *Klebsiella pneumoniae*, *Candida albicans*, *Fusarium oxysporum*, and *Aspergillus flavus*. Multiple concentrations of GO and rGO nanoparticles were tested, and it was observed that 100 $\mu g \cdot mL^{-1}$ of both GO and rGO showed the highest inhibitory effect against bacterial and produced zones of inhibition of 17.66 mm, 18.67 mm, and 17.88 for *E. coli, S. aureus, K. pneumoniae* and 20.33, 22.45, and 21.34 mm for *C. albicans, F. oxysporum,* and *A. flavus*. Comparatively, GO performed well as compared to rGO regarding antimicrobial activity. The synthesized nanoparticles exhibited significant antimicrobial activity against various bacterial and fungal strains and have the potential to be developed as novel antimicrobial agents.

Keywords: nanotechnology, green method, antimicrobial potential, graphene oxide nanoparticles

* Corresponding author: Fozia Abasi, Department of Botany, PMAS-Arid Agriculture University Rawalpindi, Rawalpindi, 46300, Pakistan, e-mail: abasifozia@gmail.com

Anila Ashraf: Department of Zoology, Women University of Azad Jammu and Kashmir, Bagh, Pakistan

Muhammad Altaf: Institute of Forest Sciences, The Islamia University of Bahawalpur, Bahawalpur, Punjab, Pakistan, e-mail: altaf_mughal450@yahoo.com

Muhammad Shahbaz: Institute for Tropical Biology and Conservation (ITBC), Universiti Malaysia Sabah, 88400, Kota Kinabalu, Malaysia, e-mail: MUHAMMAD_SHABAZ_DX22@iluv.ums.edu.my

Tanveer Hussain: Institute of Forest Sciences, The Islamia University of Bahawalpur, Bahawalpur, Punjab, Pakistan, e-mail: dr.tanveer@iub.edu.pk

Md. Arshad Ali: Biotechnology Program, Faculty of Science and Natural Resources, Universiti Malaysia Sabah, Jalan UMS, Kota Kinabalu 88400, Sabah, Malaysia, e-mail: mdarshad.ali@ums.edu.my

Jaya Seelan Sathiya Seelan: Institute for Tropical Biology and Conservation (ITBC), Universiti Malaysia Sabah, 88400, Kota Kinabalu, Malaysia

Baber Ali: Department of Plant Sciences, Quaid-i-Azam University, Islamabad, 45320, Pakistan, e-mail: baberali@bs.qau.edu.pk

Maged Mostafa Mahmoud: King Fahd Medical Research Centre, King Abdulaziz University, Jeddah, Saudi Arabia; Department of Medical Laboratory Sciences, Faculty of Applied Medical Sciences, King Abdulaziz University, Jeddah, Saudi Arabia, e-mail: mamostafa@kau.edu.sa

Steve Harakeh: King Fahd Medical Research Centre, King Abdulaziz University, Jeddah, Saudi Arabia; Yousef Abdul Latif Jameel Scientific Chair of Prophetic Medicine Application, Faculty of Medicine, King Abdulaziz University, Jeddah, Saudi Arabia, e-mail: sharakeh@gmail.com

Muhammad Hamzah Saleem: Office of Academic Research Office of VP for Research & Graduate Studies, Qatar University, Doha, 2713, Qatar, e-mail: saleemhamza312@gmail.com

1 Introduction

In the current era, nanotechnology has a wide range of applications, producing tiny nanoparticles with diameters between 1 and 100 nm, which are crucial for the treatment of many diseases [1–3]. Due to their large surface-to-volume ratio and high surface energies, these particles have a variety of biomedical purposes [4,5]. Nanoparticles (NPs) are among the most frequently produced and used

particles due to their outstanding properties, including their antibacterial and antioxidant activities, biocompatibility, and optical-polarizability [6]. In terms of catalysts, antimicrobials, antioxidants, memory aids, and cancer therapies, nanoparticles have a promising effect over other substances like Zn, Fe, Mn, Se, Cu, Ag, and Si [7]. Antimicrobial resistance represents a substantial and escalating global challenge necessitating novel strategies for addressing infections induced by antibiotic-resistant bacterial strains [8,9]. Metallic nanoparticles such as silver (Ag), gold (Au), copper oxide (CuO), iron oxide (Fe_3O_4), titanium oxide (TiO_2), or zinc oxide (ZnO) are frequently employed as antimicrobial agents due to their established potent antimicrobial activity [10]. Numerous investigations have demonstrated the biocidal efficacy of diverse metal and metal oxide nanoparticles against Gram-positive and Gram-negative bacteria, fungi, and viruses [1,11]. The antimicrobial properties of metallic nanoparticles are profoundly influenced by their elevated specific surface area, high surface-to-volume ratio, and nanoscale dimensions, facilitating robust interactions with microorganism membranes. This interaction results in membrane disruption, cellular penetration, and subsequent damage to internal cellular structures, ultimately culminating in cell demise [12].

Graphene is a carbon-based material consisting of a single layer of sp2-bonded atoms with exceptional properties such as high surface area ($2,630\ m^2{\cdot}g^{-1}$), high electrical conductivity ($2,000\ S{\cdot}cm^{-1}$), high thermal conductivity ($4,840–5,300\ W{\cdot}m^{-1}{\cdot}K^{-1}$), high electronic carrier mobility ($200,000\ cm^2{\cdot}V^{-1}{\cdot}s^{-1}$), and high Young's modulus (10 TPa) [13–16]. These properties make graphene a potential material for a wide range of applications. Graphene oxide (GO) is a modified form of graphene that contains extra oxygen functional groups, including epoxides, hydroxyl, carboxyl, and carbonyl groups on its edges and basal planes. GO-based coatings have been investigated for their potential to enhance the antibacterial properties of titanium implants [17–20]. The negatively charged and hydrophilic nature of GO facilitates interaction with osteoblasts, making it a promising material for implant applications. The sharp edges of GO can cause damage to the outer membranes of bacterial cells, as observed in studies on the antibacterial properties of GO and hydroxyapatite composites [20,21].

Studies have shown that both GO and reduced graphene oxide (rGO) possess antibacterial properties and can disrupt bacterial cell membranes with their sharp edges [21]. GO and rGO containing oxygen functional groups can oxidize glutathione, a redox mediator in bacteria, and thus reduce bacterial growth. rGO has been found to possess higher oxidation capacity than GO, graphite, and graphite oxide [22].

The emergence of multidrug-resistant microorganisms has become a major global health concern, necessitating the development of novel therapeutic strategies. Antimicrobial materials can be used to prevent microbial contamination and pathogen transmission in various settings, such as biomedical instruments and food delivery containers [23–26].

Graphene materials are advantageous than traditional antibiotics due to physical action mechanisms which contribute to decreased chances of microbial resistance. The surface oxygen content variation of these materials is the key factor for the antibacterial activity [27]. Therefore, the present study was conducted to synthesize the GO and rGO nanoparticles, and to check their antimicrobial activity against selected fungal and bacterial strains.

1.1 Preparation of extract

The lemon juice extract was prepared by acquiring fresh lemons from the local market in District Bagh, Azad Jammu and Kashmir, Pakistan. Thorough cleaning and squeezing yielded 40 mL of juice, subsequently heated for 10 min, filtered, and diluted with distilled water to produce 50 mL. To enhance reproducibility, the method involved rigorous standardization, encompassing consistent extraction protocols. The resulting mixture underwent additional stirring for 15 min at room temperature, followed by filtration. This extract was then combined with a solution of 4.7 g $KMnO_4$ in 100 mL water, acidified with 2.5 $mol{\cdot}L^{-1}$ H_2SO_4. After an hour of vigorous stirring, the purple color of the $KMnO_4$ solution transformed to black, indicating a complete reduction by the lemon juice extract. The ensuing precipitate was isolated, washed thoroughly to eliminate potassium ions, and subsequently dried overnight at 90°C, followed by calcination at 300–400°C for 5 h under ambient atmosphere [28].

1.2 Synthesis of GO

GO was prepared using 5 g of graphite and 2.5 g of sodium nitrate into 120 mL of 95% H_2SO_4. The resultant solution was placed in an ice bath, stirred for 30 min, and 15 g of potassium permanganate was added with stirring at less than 20°C temperatures. After that 150 mL of distilled water was added slowly and the solution on a magnetic stirrer overnight. After increasing the temperature from 20 to 98°C, 30% hydrogen peroxide was added to the solution. The product was washed using 5% methanolfollowed with distilled water. Finally, the product was obtained after drying.

Reduction of GO: GO 80 mg was mixed with 50 mL of distilled water and subjected to sonication for 40 min at 30°C temperature. Finally, lemon juice extract was added into the solution and refluxed for 45 min. At this stage, GO changed into rGO, which is washed with distilled water, dried, and stored at 4°C for further use [28,29].

1.3 Characterization

In this study, UV–visible spectroscopy was utilized to confirm the synthesis of GO and rGO. The morphology and size of the GO nanoparticles were examined using scanning electron microscopy (SEM), which involved the acquisition of images with a conventional secondary electron detector and a 10-kV electron beam. To determine the functional groups present in GO and rGO (rGO), Fourier transformed infrared spectroscopy (FTIR) was employed, with different wavelengths plotted on an FTIR graph to identify various functional groups. The crystalline nature of the synthesized GO nanoparticles was determined using X-ray diffraction (XRD) at the NCP, Islamabad, with NPs powdered samples placed on Shimadzu XRD-6000 and set in the range of 5°–50° at a 2θ angle. The average size of the nanoparticles was determined using Debye–Scherer's equation, which considers the shape factor (K), X-ray wavelength (λ), full width in radius at half maximum (β), and Bragg's angle (θ) (Table 1).

1.4 Experimental layout

1.4.1 Source of test organisms

All organisms used in this study included *Staphylococcus aureus*, Escherichia *coli*, *Klebsiella pneumoniae*, and *Candida albicans*, *Fusarium oxysporum*, and *Aspergillus flavus* were obtained from the Department of Microbiology, QAU Islamabad.

Table 1: Experimental design

Sr. no.	Treatments	Concentrations
1	T1	(Drug) 100 µg·mL^{-1}
2	T2	75 µg·mL^{-1} GO
3	T3	100 µg·mL^{-1} GO
4	T4	75 µg·mL^{-1} rGO
5	T5	100 µg·mL^{-1} rGO

1.4.2 Antifungal activity

Standard protocols were employed for media preparation in this study. To prepare 1 L of media, 39 g of PDA was dissolved in 1,000 mL of distilled water. The fungal culture was streaked onto the media, and 20 mL of the PDA media was poured into each Petri plate and solidified. Then, 25 µL of the samples were placed onto the discs. The petri plates were incubated at 25°C for 96 h. Three replications were used for all the treatments and experiments were performed in duplicate. The inhibition zone was measured in mm using a regular scale [30].

1.4.3 Antibacterial activity

In this study, bacterial growth was supported by nutrient agar media, which was prepared following standard microbiological principles. Nutrient agar and nutrient broth were separately prepared in 500-mL flasks, which were covered with aluminum foil and autoclaved at 121°C and 15 psi for 15 min. After autoclaving, the media was transferred to a laminar flow hood. Petri plates were filled with 20 mL of the media and left to solidify before incubation at 37°C for 24 h. Mueller Hinton Agar (MHA) was used for antimicrobial assays, and the inoculate of test microbes was prepared using the colony suspension method. Microbial suspensions were standardized to a concentration of 1.5×10^8 cfu·mL^{-1} by comparing with 0.5 McFarland standards. The Modified Kirby–Bauer diffusion technique was employed for antibiotic susceptibility testing. Standardized microbial saline suspensions were swabbed onto Mueller–Hinton agar (MHA) plates, and 7-mm filter paper discs impregnated with 20 µL of each nanoparticle solution were placed on the inoculated agar plates. Plates were incubated at 37°C for 24 h. Three replications were used for all the treatments and experiments were performed in duplicate. The zone of inhibition was measured after 24 h of incubation and interpreted accordingly [21].

1.4.4 Statistical analysis

The data were analyzed by using Statistics 8.1 software. All the values are mean ± standard error of three replications for all treatments of the experiments.

2 Results

The synthesis of GO nanoparticles was confirmed by the formation of a brown color. The reduction of GO resulted
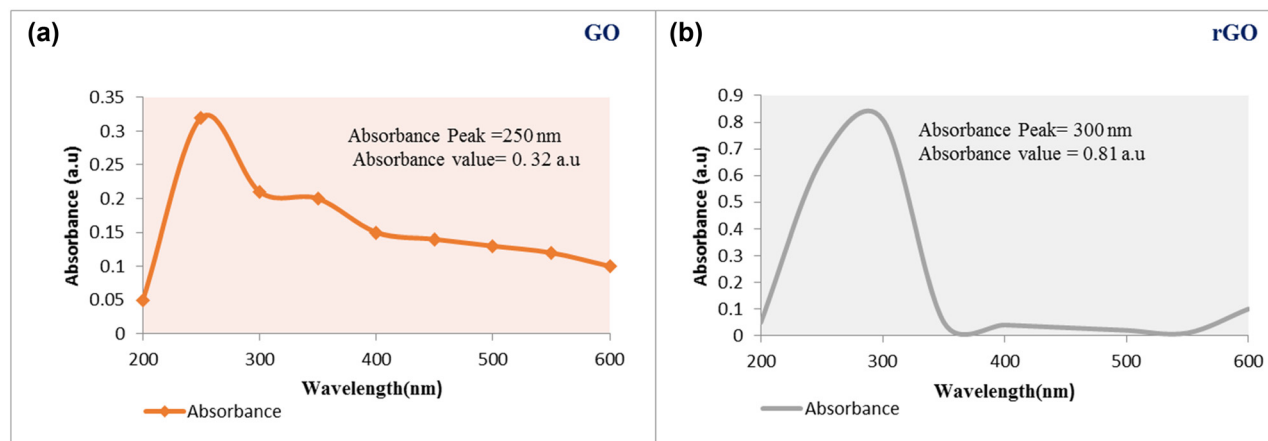
Figure 1: UV–visible spectroscopy of (a) graphene oxide and (b) reduced graphene oxide.

in the appearance of an absorbance peak at 250 nm, as depicted in Figure 1(a) and (b), indicating the successful synthesis of plant-mediated GO nanoparticles. Additionally, the UV–visible spectroscopy results of GO showed the formation of an absorbance peak at 300 nm with an absorbance value of 0.81 a.u.

SEM Analysis was employed to investigate the size and morphology of GO and rGO nanoparticles synthesized through a green synthesis method. The SEM images revealed that GO possessed a two-dimensional sheet-like morphology with multiple lamellar layers, and the edges of individual sheets were clearly distinguishable. The average size of GO and rGO nanoparticles was determined to be in the range of 60–78 and 40–58 nm, respectively. Furthermore, the SEM images showed that the films of these nanoparticles were stacked in a layered manner, resulting in the formation of wrinkled areas (Figure 2a and b). The SEM analysis of rGO obtained from GONPs demonstrated the formation of an ultra-thin Graphene film through the chemical reduction of GONPs.

To confirm the elemental composition of plant-mediated GO and rGO, an energy-dispersive X-ray (EDX) analysis was carried out. The dominant peaks in the EDX spectra for both GO and rGO were found to be in the range of 2.7–3.7 keV. Additionally, other elements such as sodium, carbon, oxygen, silver, sulfur, phosphorus, and chlorine were identified from their respective peaks in the spectra (Figure 3a and b).

The functional groups present in GO nanoparticles were characterized using Fourier Transform Infrared (FTIR) spectroscopy. The FTIR spectrum revealed the distinctive functional groups associated with GO, thereby confirming the presence of GO nanoparticles. Specifically, a broad peak at $3,306 \, cm^{-1}$, corresponding to the stretching vibration of the hydroxyl group, was observed. A sharp peak at $1,613 \, cm^{-1}$, attributed to the C=C stretching vibration, was also evident in the spectrum. Additionally, peaks at $1,222$ and $1,047 \, cm^{-1}$ were observed, which were respectively assigned to the epoxy and alkoxy groups (Figure 4a and b).

The green synthesis approach was employed for the reduction of GO nanoparticles to obtain rGO nanoparticles using lemons as a reducing agent. The rGO nanoparticles were analyzed using XRD, and characteristic peaks
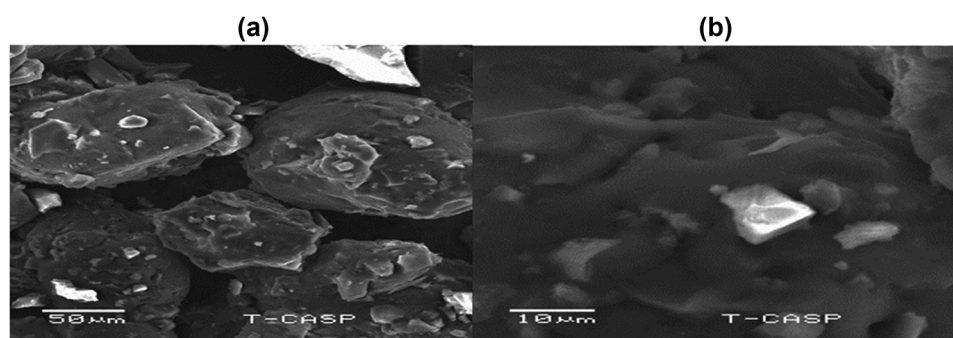
Figure 2: Scanning electron microscopy of (a) graphene oxide and (b) reduced graphene oxide.

(a)   **(b)**
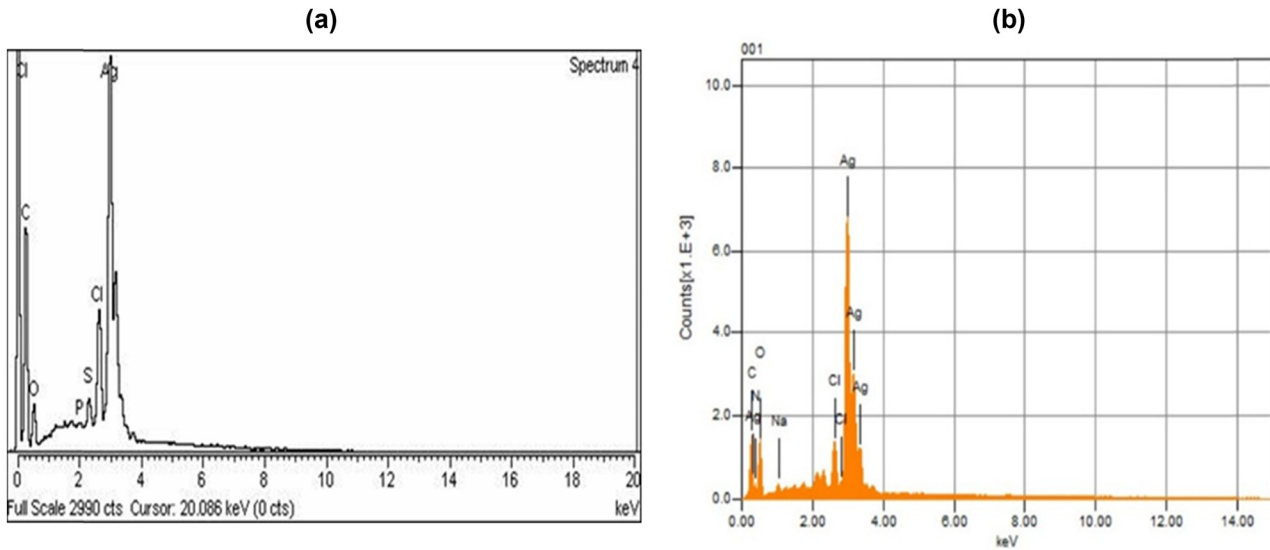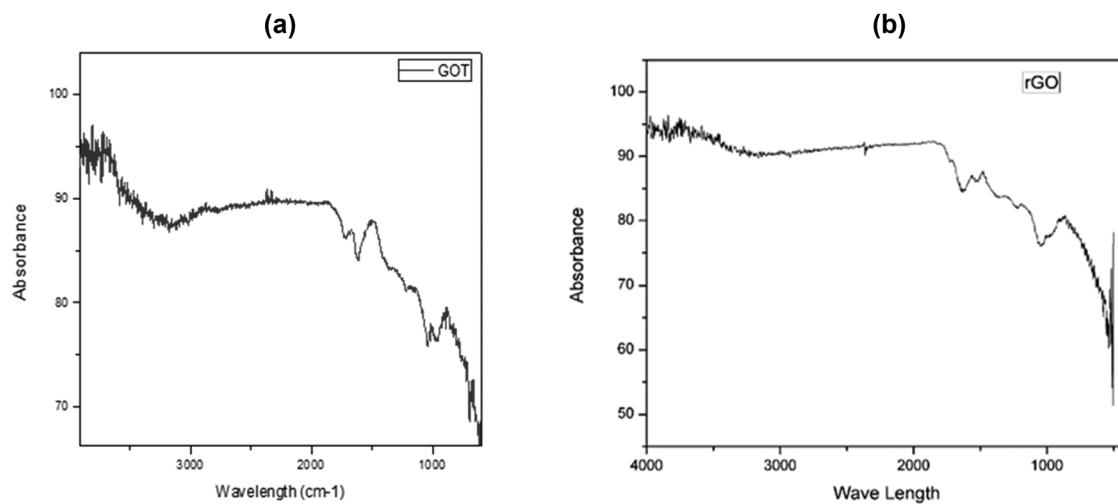

Figure 3: EDX of (a) reduced graphene oxide and (b) graphene oxide nanoparticles.

associated with rGO were observed in the XRD pattern (Figure 5a and b). Specifically, the rGO nanoparticles exhibited a distinct XRD peak at $2\theta = 30$, which is consistent with the literature values for the characteristic XRD peaks of rGO nanoparticles, typically found in the range of 26–30 theta.

The antibacterial activity of GO and rGO was evaluated against *E. coli*, *S. aureus*, and *K. pneumoniae* at concentrations of 75 and 100 µg·mL^{-1}. Streptomycin (100 µg·mL^{-1}) was used as a control. The zone of inhibition observed for rGO against *E. coli*, *S. aureus*, and *K. pneumoniae* was 17.66, 18.7, and 17.8 mm, respectively. In comparison, the zone of inhibition observed for the antibacterial drug against *E. coli*, *S. aureus*, and *K. pneumoniae* was 18, 20,

and 22 mm, respectively. Additionally, GO was tested at the same concentrations, and maximum zones of inhibition of 13.8, 16.6, and 15.3 mm were observed against *E. coli*, *S. aureus*, and *K. pneumoniae,* respectively, at a concentration of 100 µg·mL^{-1} (Figure 6). Notably, for waste treatment [23,24], the antibacterial potential of GO nanoparticles was found to be comparable to that of the antibacterial drug. These findings align with previous research conducted by Yousefi et al. [25] regarding the antibacterial activity of GO.

The antifungal activity was performed against *C. albicans*, *F. oxysporum*, and *A. flavus* using different concentrations (75 and 100 µg·mL^{-1}) of GO and rGO. The results revealed that 100 µg·mL^{-1} concentration GO and rGO performed well and produced zone of inhibition of 20.4, 22.5,

(a)   **(b)**

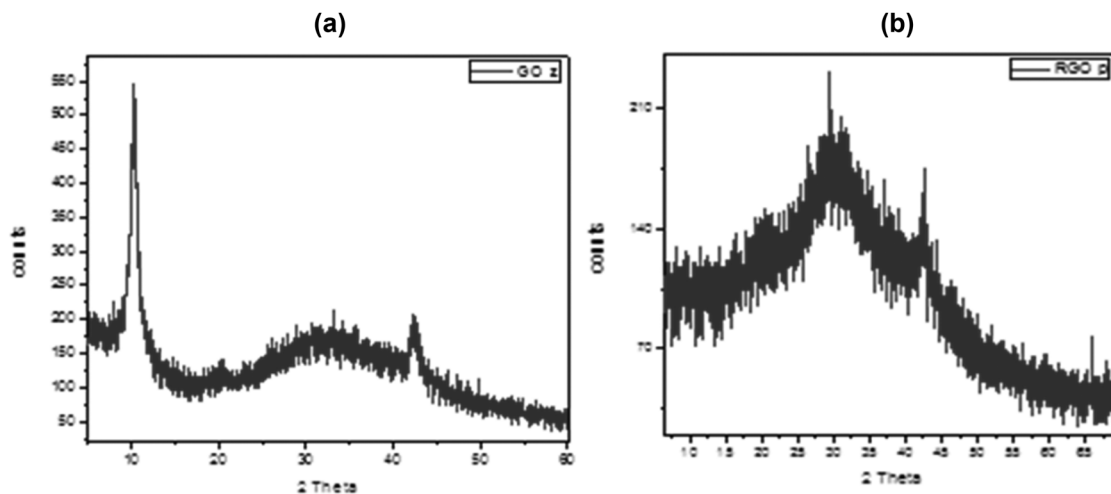**Figure 4:** FTIR spectrum of (a) graphene oxide and (b) reduced graphene oxide.

Figure 5: XRD spectrum of (a) graphene oxide and (b) reduced graphene oxide.
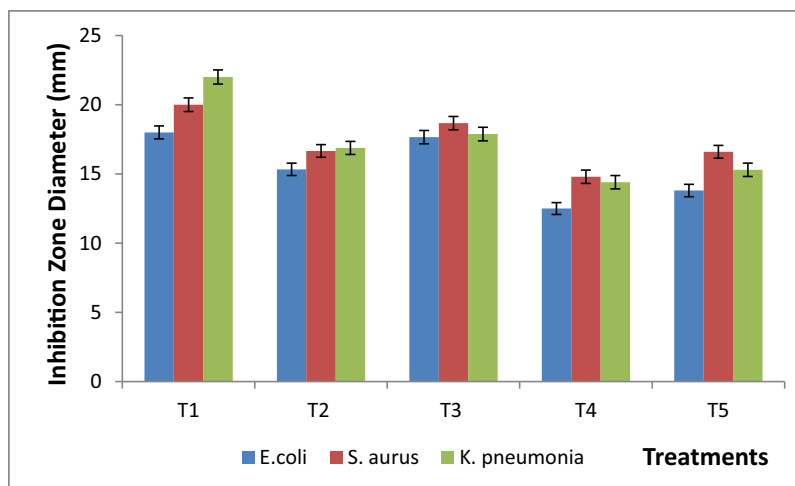

Figure 6: Effect of different concentrations of graphene oxide and reduced graphene oxide nanoparticles against selected bacterial strains.

and 21.3 mm using rGO and 17.02, 19.5, 20.2 mm using GO by comparing with antifungal drug that showed results 22.66, 23.55, and 23.78 mm of *C. albicans*, *F. oxysporum*, and *A. flavus,* respectively, as shown in Figure 7.

3 Discussion

GO and rGO are important materials in nanotechnology due to their unique properties and potential applications. The key difference between GO and rGO is the level of oxygen functionalization on the graphene surface, with GO having a higher degree of oxygen functionalization than rGO, resulting in significant changes in material properties. The UV absorption spectra of GO and rGO show a

peak at 250 and 300 nm, respectively, indicating differences in the electronic structure of the materials. GO's higher degree of oxygen functionalization leads to more oxygen-containing functional groups on the graphene surface, causing changes in the electronic structure and a shift in the UV absorption peak towards a higher wavelength. In contrast, rGO has fewer oxygen-containing functional groups due to lower oxygen functionalization, resulting in a different electronic structure and a shift in the UV absorption peak towards a lower wavelength.

Several studies have investigated the UV absorption properties of GO and rGO, with Wang et al. [31] reporting a strong absorption peak at around 300 nm for GO and a weaker peak at around 250 nm for rGO. Acik et al. [32] also observed a peak at around 300 nm for GO and a peak at around 270 nm for rGO. The difference in UV absorption
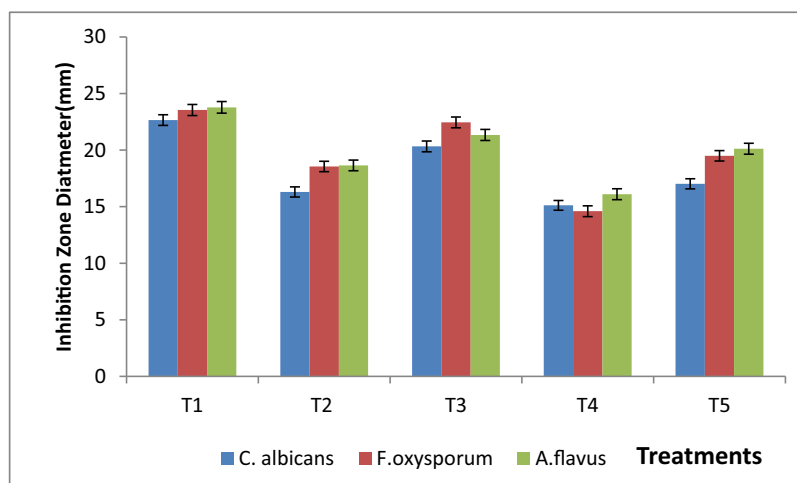
Figure 7: Effect of different concentrations of graphene oxide and reduced graphene oxide nanoparticles against selected bacterial strains.

peaks provides valuable information on the level of oxygen functionalization on the graphene surface, which can impact the material properties and potential applications.

SEM is useful for characterizing the morphology and structure of nanoparticles. The average particle size for rGO was found to be 40–58 nm, while for GO it was in the range of 60–78 nm in the results. The difference in particle size can be attributed to the different synthesis methods used to prepare GO and rGO. The synthesis method for GO involves the oxidation of graphite to form a GO precursor, which can form large sheets with many oxygen-containing functional groups, leading to larger particle sizes for the final GO product. In contrast, rGO is prepared by reducing GO, leading to the formation of smaller nanoparticles due to the removal of oxygen-containing functional groups from the GO surface. Studies by Hummers Jr and Offeman [33] and Xu et al. [34] reported particle sizes of 50–80 nm for GO and 20–40 nm for rGO, respectively, using SEM.

The EDX results indicate that rGO nanoparticles contain chlorine, phosphorus, sulfur, silver, and oxygen, while GO nanoparticles contain silver, sodium, carbon, oxygen, and phosphorus. These differences in elemental composition can be attributed to variations in the synthesis methods employed. During the oxidation process in the preparation of GO, various oxygen-containing functional groups can form, leading to the incorporation of elements such as sodium and phosphorus. Additionally, the use of silver nitrate as a catalyst in the synthesis process can explain the presence of silver in the GO sample. On the other hand, the reduction process used in the preparation of rGO can introduce impurities such as chlorine, which may arise from the use of reducing agents or surfactants. The

presence of silver in the rGO sample may be due to the use of silver ions in the reduction process.

Previous studies have also reported the elemental composition of GO and rGO nanoparticles using EDX analysis. Wang et al. [31] found oxygen, carbon, and silicon in GO nanoparticles, while rGO nanoparticles contained oxygen, carbon, and sulfur. Similarly, Zhang et al. [35] reported the presence of carbon, oxygen, and nitrogen in GO nanoparticles and carbon, oxygen, and sulfur in rGO nanoparticles.

The infrared (IR) spectra of both GO and L-cysteine reduced GO (LCrGO) were analyzed, revealing an intense absorption peak at 3,352 and 3,224 cm^{-1} that can be attributed to the OH extending vibration of the phenol or alcoholic functional group. Another absorption band was observed at 2,925 cm^{-1} in LCrGO, representing the C–H group. The absence of the carbonyl group at 1,722 cm^{-1} in LCrGO compared to GO confirmed the effective reduction of GO. The presence of C=C bond was confirmed by the appearance of a band at 1,621 cm^{-1} in GO and 1,587, 1,647 cm^{-1} in LCrGO. Similar functional groups were also reported by other researchers [36].

The GO diffraction pattern showed a prominent peak at $2\theta = 11.3°$, corresponding to the graphene oxide plate (002), and a weak peak at about $2\theta = 26.4°$, which is usually caused by unaffiliated graphite. The transformation of the GO structure due to the hydrothermal process led to the disappearance of some oxygenated groups, resulting in a prominent peak at $2\theta = 11.3°$ and a weak peak at $2\theta = 26.4°$. These findings are consistent with previous reports by Sajjad et al. [37].

Both the GO and rGO showed antagonistic activity against bacterial and fungal pathogens. The inhibition activity of antibacterial and antifungal drugs is more

than nanoparticles but it is still important to consider nanoparticles as an alternative to drugs. Microorganisms may develop resistance by limiting drug uptake, target drug modification, drug inactivation, and drug efflux [38]. The pathogenic microorganisms may develop resistance to multiple drugs, and production of these drugs is complex and costly. It is easy to synthesize nanoparticles; especially, the plant extract–oriented synthesis of nanoparticles is easy and economically affordable. So, we should consider the optimization of the biosynthesis of nanoparticles for our well-being. The GO and rGO nanoparticles have been reported to have antifungal effects by potentially invading the cell membrane and disrupting its integrity, leading to leakage of vital cell materials and cell death [39]. The Go and rGO nanomaterials produced reactive oxygen species and showed antibacterial activity against *E. coli* and *Bacillus subtilis* by surface modification of membrane filters [40]. GO and rGO nanoparticles have also been used to suppress *Alternaria alternata* causing tomato leaf blight, with a dose of 100 µg·mL^{-1} resulting in an inhibition percentage of 89.6% [41]. In addition, GO and rGO nanoparticles were applied against *Alternaria solani*, a causal agent of early blighting potatoes resulting in a 100% inhibition at a concentration of 80 ppm [42]. These findings are consistent with those reported by Whitehead et al. [43].

4 Conclusion

The objective of this study was to investigate the effectiveness of GO nanoparticles (GO NPs) against selected bacterial and fungal strains. These findings demonstrate the potential of GO NPs as effective antimicrobial agents against bacterial and fungal strains and suggest that they could be a promising candidate for the development of novel antimicrobial agents. Further, research is necessary to explore their potential clinical applications and toxicity profiles.

Author contributions: All authors of this research article have contributed significantly to the literature study, writing, and methodology, and critically revised the research article. A. A.: conceptualization/conceived the study idea, planned and designed the research structure, wrote the first draft of the manuscript, data validation, visualization, customized images, and final draft. M. A., and T. H. supervised the research, and drafting process, and revised the first draft. M.S: formal analysis, validation, resources, suggestions. F. A.: and M. I., conceptualization, data curation, review editing, software and validation, F. Y. methodology, visualization, validation, and final editing of manuscript. Funder: helped with data validation and interpretation, guided the draft write-up, and carried out a critical revision of the final draft; and funding acquisition. All authors have read and agreed to the published version of the manuscript.

Conflict of interest: The authors state no conflict of interest.

Data availability statement: All data generated or analyzed during this study are included in this published article.

References

[1] Sharmin S, Rahaman MM, Sarkar C, Atolani O, Islam MT, Adeyemi OS. Nanoparticles as antimicrobial and antiviral agents: A literature-based perspective study. Heliyon. 2021;7(3):06456.

[2] Hassan HU, Raja NI, Abasi F, Mehmood A, Qureshi R, Manzoor Z, et al. Comparative study of antimicrobial and antioxidant potential of olea ferruginea fruit extract and its mediated selenium nanoparticles. Molecules. 2022;27(16):5194.

[3] Sadiq S, Akhtar S. The efficacy of common windmill butterfly's silver nanoparticles against bacterial pathogens. J Wildl Ecol. 2023;7(2):35–43.

[4] Shahbaz M, Akram A, Raja NI, Mukhtar T, Mashwani ZUR, Mehak A, et al. Green synthesis and characterization of selenium nanoparticles and its application in plant disease management: A review. Pak J Phytopathol. 2022;34(1):189–202.

[5] Duhan JS, Kumar R, Kumar N, Kaur P, Nehra K, Duhan S. Nanotechnology: The new perspective in precision agriculture. Biotechnol Rep. 2017;15:11–23.

[6] Hatamifard A, Nasrollahzadeh M, Sajadi SM. Biosynthesis, characterization and catalytic activity of an Ag/zeolite nanocomposite for base-and ligand-free oxidative hydroxylation of phenylboronic acid and reduction of a variety of dyes at room temperature. N J Chem. 2016;40(3):2501–13.

[7] Khodadadi B, Bordbar M, Nasrollahzadeh M. Achillea millefolium L. extract mediated green synthesis of waste peach kernel shell supported silver nanoparticles: application of the nanoparticles for catalytic reduction of a variety of dyes in water. J Colloid Interface Sci. 2017;493:85–93.

[8] Salam MA, Al-Amin MY, Salam MT, Pawar JS, Akhter N, Rabaan AA. et al. Antimicrobial resistance: A growing serious threat for global public health. Healthcare. 2023;11:1946.

[9] Nazer S, Butt I, Fatima I. Antibacterial and synergistic potential of scale extracts from Oreochromis mossambicus against bacterial pathogens. J Wildl Ecol. 2023;7(1):11–9.

[10] Beyth N, Houri-Haddad Y, Domb A, Khan W, Hazan R. Alternative antimicrobial approach: Nano-antimicrobial materials. Evid-Based Complement Altern Med. 2015;2015:246012.

[11] Manzoor I, Safeer B. Synthesis of silver nanoparticles from skin of *Labeo rohita* and their application of biocide. J Wildl Ecol. 2022;6(3):129–40.

[12] Wang L, Hu C, Shao L. The antimicrobial activity of nanoparticles: present situation and prospects for the future. Int J Nanomed. 2017;12:1227–49.

[13] Novoselov KS, Geim AK, Morozov SV, Jiang D, Zhang Y, Dubonos SV, et al. Electric field effect in atomically thin carbon films. Science. 2004;306(5696):666–9.

[14] Balandin AA, Ghosh S, Bao W, Calizo I, Teweldebrhan D, Miao F, et al. Superior thermal conductivity of single-layer graphene. Nano Lett. 2008;8(3):902–7.

[15] Bolotin KI, Sikes KJ, Jiang Z, Klima M, Fudenberg G, Hone J, et al. Ultrahigh electron mobility in suspended graphene. Solid State Commun. 2008;146(9–10):351–5.

[16] Lee C, Wei X, Kysar JW, Hone J. Measurement of the elastic properties and intrinsic strength of monolayer graphene. Science. 2008;321(5887):385–8.

[17] Kim K, Ahn SI, Choi KC. Simultaneous synthesis and patterning of graphene electrodes by reactive inkjet printing. Carbon. 2014;66:172–7.

[18] Tanurat P, Sirivisoot S. Osteoblast proliferation on graphene oxide eletrodeposited on anodized titanium. Paper presented at: 2015 8th Biomedical Engineering International Conference (BMEiCON); 2015.

[19] Gu M, Lv L, Du F, Niu T, Chen T, Xia D, et al. Effects of thermal treatment on the adhesion strength and osteoinductive activity of single-layer graphene sheets on titanium substrates. Sci Rep. 2018;8(1):8141.

[20] Zhu Y, Murali S, Cai W, Li X, Suk JW, Potts JR, et al. Graphene and graphene oxide: Synthesis, properties, and applications. Adv Mater. 2010;22(35):3906–24.

[21] Liu S, Zeng TH, Hofmann M, Burcombe E, Wei J, Jiang R, et al. Antibacterial activity of graphite, graphite oxide, graphene oxide, and reduced graphene oxide: membrane and oxidative stress. ACS Nano. 2011;5(9):6971–80.

[22] Hu W, Peng C, Luo W, Lv M, Li X, Li D, et al. Graphene-based antibacterial paper. ACS Nano. 2010;4(7):4317–23.

[23] Burduşel A-C, Gherasim O, Grumezescu AM, Mogoantă L, Ficai A, Andronescu E. Biomedical applications of silver nanoparticles: An up-to-date overview. Nanomaterials. 2018;8(9):681.

[24] Habib S. Antibacterial activity of biogenic synthesized silver nanoparticles using skin of Kashmir Nadi Frog Paa barmoachensis. J Wildl Ecol. 2022;6(1):07–12.

[25] Yousefi N, Wong KKW, Hosseinidoust Z, Sørensen HO, Bruns S, Zheng Y, et al. Hierarchically porous, ultra-strong reduced graphene oxide-cellulose nanocrystal sponges for exceptional adsorption of water contaminants. Nanoscale. 2018;10:7171–84.

[26] Zainab S. Antibacterial and antibiofilm activity of Bull frog *Hoplobatrachus tigerinus* skin extract. J Wildl Ecol. 2021;5:32–7.

[27] Guo Z, Zhang P, Xie C, Voyiatzis E, Faserl K, Chetwynd AJ, et al. Defining the surface oxygen threshold that switches the interaction mode of graphene oxide with bacteria. ACS Nano. 2023;17(7):6350–61.

[28] Hashem AM, Abuzeid H, Kaus M, Indris S, Ehrenberg H, Mauger A, et al. Green synthesis of nanosized manganese dioxide as positive electrode for lithium-ion batteries using lemon juice and citrus peel. Electrochim Acta. 2018;262:74–81.

[29] Aunkor M, Mahbubul I, Saidur R, Metselaar H. The green reduction of graphene oxide. RSC Adv. 2016;6(33):27807–28.

[30] Wareen G, Saeed M, Ilyas N, Asif S, Umair M, Sayyed RZ, et al. Comparison of pennywort and hyacinth in the development of membraned sediment plant microbial fuel cell for waste treatment. Chemosphere. 2023;313:137422.

[31] Wang X, Sun G, Routh P, Kim D-H, Huang W, Chen P. Heteroatom-doped graphene materials: syntheses, properties and applications. Chem Soc Rev. 2014;43(20):7067–98.

[32] Acik M, Mattevi C, Gong C, Lee G, Cho K, Chhowalla M, et al. The role of intercalated water in multilayered graphene oxide. ACS Nano. 2010;4(10):5861–8.

[33] Hummers Jr WS, Offeman RE. Preparation of graphitic oxide. J Am Chem Soc. 1958;80(6):1339–9.

[34] Xu Y, Bai H, Lu G, Li C, Shi G. Flexible graphene films via the filtration of water-soluble noncovalent functionalized graphene sheets. J Am Chem Soc. 2008;130(18):5856–7.

[35] Zhang P, Wang H, Zhang X, Xu W, Li Y, Li Q, et al. Graphene film doped with silver nanoparticles: self-assembly formation, structural characterizations, antibacterial ability, and biocompatibility. Biomater Sci. 2015;3(6):852–60.

[36] Navaee A, Salimi A. Efficient amine functionalization of graphene oxide through the Bucherer reaction: an extraordinary metal-free electrocatalyst for the oxygen reduction reaction. RSC Adv. 2015;5(74):59874–80.

[37] Sajjad M, Ahmad F, Shah LA, Khan M. Designing graphene oxide/silver nanoparticles based nanocomposites by energy efficient green chemistry approach and their physicochemical characterization. Mater Sci Eng: B. 2022;284:115899.

[38] Reygaert WC. An overview of the antimicrobial resistance mechanisms of bacteria. AIMS Microbiol. 2018;4(3):482–501.

[39] Collado IG, Aleu J, Macías-Sánchez AJ, Hernández-Galán R. Synthesis and antifungal activity of analogues of naturally occurring botrydial precursors. J Chem Ecol. 1994;20:2631–44.

[40] Ismail A-W, Sidkey N, Arafa R, Fathy R, El-Batal A. Evaluation of in vitro antifungal activity of silver and selenium nanoparticles against Alternaria solani caused early blight disease on potato. Br Biotechnol J. 2016;12(3):1–11.

[41] Musico YLF, Santos CM, Dalida MLP, Rodrigues DF. Surface modification of membrane filters using graphene and graphene oxide-based nanomaterials for bacterial inactivation and removal. ACS Sustain Chem Eng. 2014;2:1559–65.

[42] Feng R, Wei C, Tu S. The roles of selenium in protecting plants against abiotic stresses. Environ Exp Bot. 2013;87:58–68.

[43] Whitehead K, Vaidya M, Liauw C, Brownson D, Ramalingam P, Kamieniak J, et al. Antimicrobial activity of graphene oxide-metal hybrids. Int Biodeterior Biodegradation. 2017;123:182–90.